CHIN. PHYS. LETT. Vol. 38, No. 6 (2021) 063101

Multi-Electron Transfer of Ar^+ Colliding with Ne Atoms Based on a Time-Dependent Density-Functional Theory

Shuai Qin(秦帅)[1], Cong-Zhang Gao(高聪章)[2], Wandong Yu(于皖东)[3*], and Yi-Zhi Qu(屈一至)[1*]

[1]*School of Optoelectronics, University of Chinese Academy of Sciences, Beijing 100049, China*
[2]*Institute of Applied Physics and Computational Mathematics, Beijing 100088, China*
[3]*State Key Laboratory for Mesoscopic Physics and Frontiers Science Center for Nano-optoelectronics, School of Physics, Peking University, Beijing 100871, China*

(Received 10 February 2021; accepted 19 March 2021; published online 25 May 2021)

The multi-electron capture and loss cross-sections of Ar^+–Ne collisions are calculated at absolute energies in the few-keV/a.u. regime. The calculations are performed using a novel inverse collision framework, in the context of a time-dependent density functional theory, combined with molecular dynamics. The extraction of the capture and loss probabilities is based on the particle-number projection technique, originating from nuclear physics, but validly extended to represent many-electron systems. Good agreement between experimental and theoretical data is found, which clearly reveals the non-negligible post-collision decay of the projectile's electrons, providing further evidence for the applicability of the approach to complex many-electron collision systems.

DOI: 10.1088/0256-307X/38/6/063101

Charge-transfer processes in ion collisions have been studied extensively for many years (for a recent review, see Refs. [1,2], and references therein). They are of great interest in many research fields, such as plasma diagnostics,[3] astrophysics,[4–6] radiation medicine,[7] and in particular, in current projects related to cross-section measurement involving partially stripped ion beams, where the charge-changing of the dressed projectile ions can give rise to a non-negligible impact on the measured cross-sections, of varying orders of magnitude. From the more fundamental perspective of atomic physics, these collision systems have attracted considerable attention,[8–11] as many different processes, e.g., charge-transfer excitation, ionization, post-collision interactions, and electron transfer, can occur and take effect, and further interesting phenomena are expected, with respect to electronic dynamics. Despite the importance of charge-transfer processes in dressed-ion collisions, their theoretical description remains challenging: the screening effects of active electrons in the dressed projectile have not yet been adequately described, and more importantly, the role of electronic loss of the dressed projectile in relation to charge-transfer dynamics needs to be clearly demonstrated.[12–14]

In terms of the quantum-mechanical modeling of dressed ion collisions, methods based on the independent electron approximation (IEA) have been applied with some success. Kirchner and coworkers proposed a coupling mean-field approach to describe initial electronic states, based on an IEA model, which has been applied to certain dressed-ion collisions.[8,15–17] For instance, using an IEA model in which both projectile's and target's active electrons are propagated in a common mean-field potential, Schenk *et al.* demonstrated that net recoil-ion production via fully stripped ion impact exceeds that of a dressed ion.[15] In addition, it is worth mentioning that close-coupling treatments[18] can be used in a description of charge transfer in dressed-ion collisions. In a highly relevant work by Imai *et al.*,[19] single- and double-charge transfer cross sections of Ne^{2+}-He collision below 10 keV/a.u. were studied using the molecular-orbital close-coupling method (MOCC; it was found that excited states in the dressed projectile play a key role in charge-transfer processes. Alternate theoretical methods include that based on two-center atomic orbital expansions, as employed by Kirchner *et al.*,[20] quantum-mechanical molecular-orbital close-coupling (QMOCC) method by Wang *et al.*,[21] or the atomic orbital close-coupling (AOCC) approach of Gao *et al.*[22] However, to the best of our knowledge, these previous methods have not yet been successfully extended to include more complicated collision systems, such as the Ar^+–Ne collision with 15 electrons covered here, or other ion–molecule collisions. Owing to its computational efficiency and size scalability, the time-dependent density-functional theory (TDDFT),[23,24] combined with non-adiabatic molecular dynamics (MD), has been selected in a number of previous studies to simulate ion-atomic/molecular/solid collisions.[25–28] In this work, based on TDDFT-MD, we investigate a prototypical system of Ar^+–Ne collision in the energy

Supported by the National Key Research and Development Program of China (Grant No. 2017YFA0402300), and the National Natural Science Foundation of China (Grant Nos. 11774344, 11704039, 11774030, and 11704037).
*Corresponding authors. Email: wandongyu@pku.edu.cn; yzqu@ucas.edu.cn
© 2021 Chinese Physical Society and IOP Publishing Ltd

region of 1.6 keV/a.u. to 45 keV/a.u., by comparing our calculated results to those of experimental data, which have not yet been extensively analyzed. The collision of Ar^+ ions with Ne atoms is of great importance in the field of astrophysics, where the valence electrons of the dressed Ar^+ ion are predominantly responsible for various phenomena in the solar corona and aurora.[29–32] Compared to fully stripped projectile ions, Pivovar *et al.*[33] have demonstrated that the dressed Ar^+ ion induces a more sensitive dependence in relation to charge-transfer cross sections on impact energies ranging in 6.3–45 keV/a.u. Although the classical-trajectory Monte–Carlo method has been applied to examine single- and multiple-electron loss cross-sections in heavy ions relating to atomic and molecular targets for high impact energies above 1 MeV/a.u.,[34–36] it fails at intermediate and low energies, due to significant overestimations of electronic loss cross-sections. By combining it with a statistical theory for the projectile's ionization probability, Shevelko *et al.*[37] proposed an improved classical energy-deposition model to describe the role of electronic loss in Ar^+ ions in collision with Ne, leading to quite reasonable results with respect to ionization cross-sections. The above endeavors indicate the significance of electronic loss in a projectile, with respect to charge-transfer dynamics and cross-sections.

In this Letter, we discuss how electron capture and loss cross-sections in Ar^+–Ne collisions can be effectively computed within the TDDFT. Our results show that electron loss in the Ar^+ projectile plays a key role in charge-transfer dynamics as well as probabilities; to the best of our knowledge, Ar^+–Ne collision has not yet been studied at the quantitative level in this specific energy region. The electron dynamics of the Ar^+ ion reveal a violent electron loss after collision, followed by a sustained ionization, lasting for hundreds of femtoseconds. The cross-sections of single electron capture and electron loss are in agreement with both existing theory and the available experimental data.

The Ar^+–Ne collision is performed within TDDFT-MD, in which the ionic dynamics is classically described by the Ehrenfest theorem, and the single-electron wavefunctions are quantum-mechanically described via time-dependent Kohn–Sham (TDKS) equations:[23,24,38–41]

$$i\frac{\partial}{\partial t}\Psi_i(\boldsymbol{r},t) = [-\frac{1}{2}\nabla^2 + V_{\rm ks}[\rho](\boldsymbol{r},t)]\Psi_i(\boldsymbol{r},t), \quad i=1,2,\ldots,N, \tag{1}$$

$$M_j\frac{\partial^2}{\partial t^2}\boldsymbol{R}_j(t) = -\nabla_{\boldsymbol{R}_j}\left[\int d^3\boldsymbol{r}\rho(\boldsymbol{r},t)V_{\rm en}[\{\boldsymbol{R}_j(t)\},\boldsymbol{r}] + \sum_{j\neq j'}^{N_n}\frac{z_j z_{j'}}{|\boldsymbol{R}_j(t)-\boldsymbol{R}_{j'}(t)|}\right], \tag{2}$$

where i is the ith Kohn–Sham orbital (KSO), and R_j denotes the coordinates of the jth ion. The effective KS potential consists of Hartree potential, exchange-correlation potential, and the electron-ion potential, $V_{\rm en}$. Here, N and N_n are the total numbers of electrons and ions, respectively. TDDFT-MD, which achieves an acceptable balance between computational efficiency and the accuracy of its results, has been successfully applied to the description of charge-transfer processes in ion-atom/molecule collisions over a wide energy range,[42,43] such as He^+–He,[8] H^+–He,[44] H^+–N_2,[45,46] and Ar^{8+}–C_2H_2.[47] In terms of the Ar^+–Ne collision considered in this work, we emphasize that only 15 valence electrons are considered, i.e., 8 electrons ($2s^22p^6$) from the outermost shell of the Ne atom, and 7 electrons ($3s^23p^5$) from that of the Ar^+ ion. The remaining inner-shell electrons are frozen, and experience any effects via norm-conserving pseudopotentials. To extract the capture/loss probability as accurately as possible, the TDDFT-MD calculations are performed in an inverse collision framework, in which the Ar^+ ion, depicted as the target, is initially stationary, and the Ne atom is boosted as the projectile. Initially, both Ar^+ ion and Ne atom exist in their ground states, and a phase factor, $e^{i\boldsymbol{v}\cdot\boldsymbol{r}}$, is added in front of each KSO of the Ne atom to boost its electronic density, moving with the velocity, $\boldsymbol{v}$. The phase factor, commonly known as the electron translation factor,[48] causes the KSOs of the Ne atom to carry an additional linear momentum as well as a kinematic energy, avoiding non-traveling states in the Ne atom. It is convenient to use the inverse collision framework[49] in order to obtain the converged KSOs associated with the Ar^+ ion, given that in the normal collision framework (i.e., the Ar^+ ion is the projectile impinging on the Ne atom), these KS orbitals are lost once the Ar^+ is scattered out of the computational box. The electron capture and loss probabilities of the Ar^+ ion, extracted by applying particle number projection method (PNP), are determined by the spatial partition of the electrons.[50] Specifically, the n-electron capture (or loss) probability of the Ar^+ ion is defined by the probability that $7+n$ (or $7-n$) electron exist in the capture region of the Ar^+ ion, i.e., the region V_τ, as shown in Fig. 1. Assuming that the total wavefunction of the collision system is a single slater determinant, comprising the occupied KSOs, the n-electron capture, $P_n^{\rm cap}$, and m-electron loss, the $P_m^{\rm loss}$ probability of the Ar^+ ion can be expressed as

$$P_n^{\rm cap} = \sum_{\{s_i|V_\tau^{7+n}V_{\bar\tau}^{N-(7+n)}\}}\det\{\langle\psi_i\,|\,\psi_j\rangle_{s_i}\}, \tag{3}$$

$$P_m^{\rm loss} = \sum_{\{s_i|V_\tau^{7-m}V_{\bar\tau}^{N-(7-m)}\}}\det\{\langle\psi_i\,|\,\psi_j\rangle_{s_i}\}, \tag{4}$$

where $V_{\bar\tau}$ is the complementary region of V_τ. The notation $\{s_i|V_\tau^kV_{\bar\tau}^{N-k}\}$ means that the sum should be taken for all possible species combinations, s_i, that in

the sequence s_1, $s_2, \ldots, s_N$, k electrons bounded in V_τ, and all the other electrons bounded in $V_{\bar{\tau}}$. The overlap in the determinant is calculated by

$$\langle \psi_i \,|\, \psi_j \rangle_{s_i} \equiv \int_{s_i} \psi_i^*(\boldsymbol{x}) \psi_j(\boldsymbol{x}) d\boldsymbol{x}, \tag{5}$$

where $\boldsymbol{x}$ denotes the spatial and spin coordinates, respectively. Based on the orthogonality of the KSOs for the whole space, the overlap in V_τ or $V_{\bar{\tau}}$ satisfies

$$\langle \psi_i \,|\, \psi_j \rangle_{V_\tau} \equiv \delta_{ij} - \langle \psi_i \,|\, \psi_j \rangle_{V_{\bar{\tau}}}. \tag{6}$$

Finally, for the incident energy, E, the n-electron capture, $\sigma_n^{\rm cap}$, and the m-electron loss $\sigma_m^{\rm loss}$ cross-sections are calculated by the integral over the impact parameters:

$$\sigma_n^{\rm cap} = 2\pi \int_{b_{\rm min}}^{b_{\rm max}} dbbP_n^{\rm cap}(E, b), \tag{7}$$

$$\sigma_m^{\rm loss} = 2\pi \int_{b_{\rm min}}^{b_{\rm max}} dbbP_m^{\rm loss}(E, b). \tag{8}$$

All calculations are performed using the OCTOPUS program,[51–53] and the parameters below ensure the numerical stability. The size of the computational box is $(66 \times 39 \times 26)\ a_0^3$, with a spacing of $0.4a_0$. As shown in Fig. 1, the Ar^+ ion is initially placed at $(0.0,\ -6.5,\ 0.0)a_0$, and the Ne atom is initially at $(-20.0,\ -6.5 + b,\ 0.0)a_0$. The impact parameter is denoted as b, ranging from $0.5a_0$ to $7.5a_0$, with a step of $0.5a_0$. The time step is 0.02 a.u. The many-electron exchange-correlation effects are described using the Perdew–Zunger adiabatic local density approximation, together with the Perdew–Zunger self-interaction correction,[54] and the core electron effects via a norm-conserving pseudopotential.[55] The total propagation time is longer than 242 fs, at which the final KSOs are stably converged. The ionic motion is propagated by the velocity Verlet algorithm.[56,57] The absorbing boundary, described by a $\cos^2$ mask function[58] with a width of $3a_0$, is used to remove the reflection of electronic orbitals. The region V_τ is selected as the whole computational box, which is numerically large enough to include the final KSOs associated with the Ar^+ ion.

Figure 2 illustrates the two-dimensional integral electronic density inside the computational box at $b = 3a_0$ for four impact energies in the considered energy region, i.e., 6.3, 10, 25, and 45 keV/a.u. Over time, the ionized electrons reach the edges of the computational box, and are then absorbed by the absorbing boundary. Note that the captured electronic density cannot be clearly observed, owing to the fact that the initial electronic density on the Ne atom is far greater. Here, we present 4 different impact energies in order to illustrate the energy effects on Ar^+ ionization, as well as the subsequent electron-ion dynamics. As the impact energy increases, a more violent electronic excitation is observed within a few femtoseconds. This collision-excitation process results in the density evolution of the Ar ion being highly nonlocal. After a lengthy time propagation, generally more than 240 fs, the density of the Ar ion becomes relatively stable. It is therefore necessary to evolve the post-collision system over long time scales, i.e., hundreds of femtoseconds, in order to achieve the converged results.

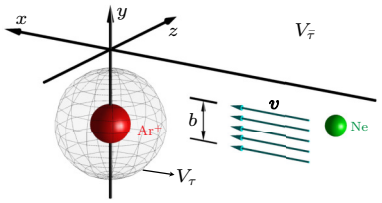

Fig. 1. Schematic diagram of Ar^+–Ne collision in the inverse collision framework. The big red ball represents the target Ar^+ ion, and the small green ball is the incident Ne atom. V_τ is the capture region of the Ar^+ ion. Cyan arrows denote the impact direction.

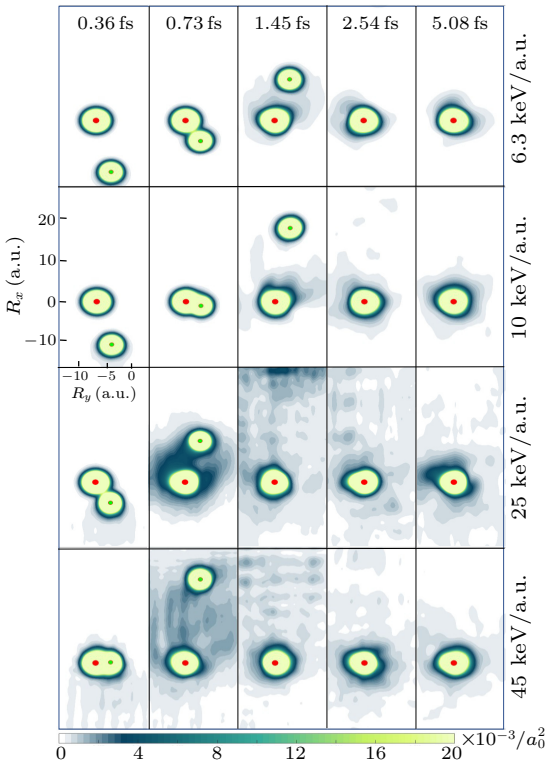

Fig. 2. Snapshots of two-dimensional integral electronic density inside the computational box for Ar^+–Ne collision at 6.3, 10, 25, and 45 keV/a.u., for a sequence of snapshots. The impact parameter is $3a_0$. The red dot represents the Ar nuclei, and the green dot is the Ne nuclei.

Figure 3 shows the electron capture cross-section ($\sigma_n^{\rm cap}$, $n = 1$), electron loss cross-sections ($\sigma_m^{\rm loss}$, $m = 1, \ldots, 5$), and total electron loss cross-section ($\sigma_{\rm tot} = \sum_{m=1}^{7} \sigma_m^{\rm loss}$) for incident energies from 1.6 keV/a.u. to 45 keV/a.u. The results are compared with available experimental data, together with existing theo-

retical results. With respect to the capture process for a single electron, the cross-sections, both theoretical and experimental, decrease with an increase in impact energy, where the impact energy is greater than 6.3 keV/a.u. [see Fig. 3(a), which indicates that the electron capture process is more likely to occur at lower energy region]. Our calculations are within the error range of the experimental data of Pivovar *et al.*[33] for incident energy levels greater than 25 keV/a.u. However, there is an obvious deviation between the experimental data of Pivovar *et al.*[33] and that of Wittkower *et al.*[59] in the range from 1.6 keV/a.u. to 12.5 keV/a.u. Specifically, the results obtained in our calculations lie between those of Pivovar *et al.*[33] and Wittkower *et al.*[59] In this context, it is difficult to say more in regard to the experimental data within the energy range considered in this work; further theoretical calculations and experiments would be required to validate the single charge-transfer cross-sections for the collision of argon ions and neon atoms.

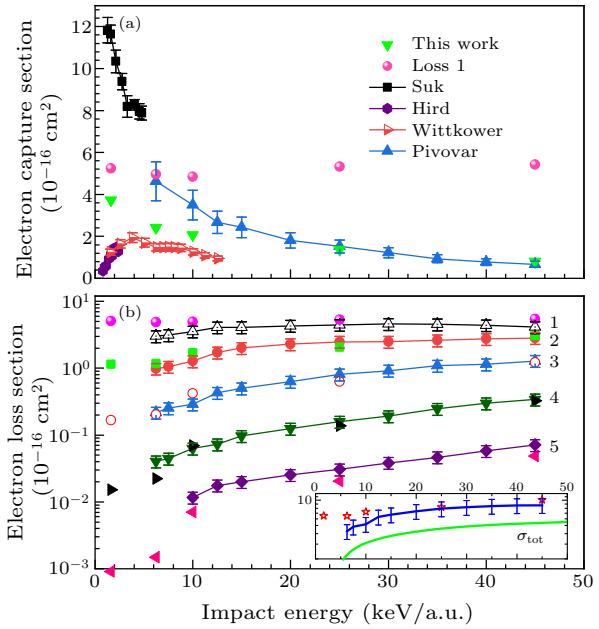

Fig. 3. Electron capture cross-section ($\sigma_n^{\rm cap}$, $n = 1$), electron loss cross-section ($\sigma_m^{\rm loss}$, $m = 1,\ldots,5$), and total electron loss cross section ($\sigma_{\rm tot} = \sum_{m=1}^{7} \sigma_m^{\rm loss}$), as a function of the incident energies. (a) Experimental data: Suk *et al.* (black line, denoting the single-electron capture cross-section of Ar^{2+} impact with Ne), Hird *et al.* (purple line), Wittkower *et al.* (red line), Privovar *et al.* (blue line), this work: single electron capture (green triangles), single electron loss (magenta balls). (b) Experimental data: Privovar *et al.* (lines, correspond to $\sigma_m^{\rm loss}$, $m = 1,\ldots,5$, from top to bottom). Theory: this work: (spot, corresponding to $\sigma_m^{\rm loss}$, $m = 1,\ldots,5$, from top to bottom). The inset represents the total loss cross-section: this work (red dot), Privovar *et al.* (blue line), Shevelko *et al.* (green line).

Figure 3(b) shows the multi-electron loss cross-sections, $\sigma_{m=1-5}^{\rm loss}$, as a function of the impact energy. The calculated $\sigma_{m=1-4}^{\rm loss}$ agrees with the experimental data, and the $\sigma_{m=5}^{\rm loss}$ is slightly lower. In contrast to the single-electron capture cross-sections, the single-electron loss cross-sections are almost independent of the impact energy, and the multi-electron loss cross-sections, $\sigma_{m=3-5}^{\rm loss}$, increase monotonically with the increase in impact energy. This energy-dependence reflects the fact that electron-loss processes prefer higher impact energies, and that the violent ionization at high impact energies may be significant in facilitating electron-loss probabilities. When the incident energy of a single-electron loss process is below 6.3 keV/a.u., there is an obvious distinction between the calculated electron loss cross-sections and the experimental results, in that the cross-section actually increases with a decrease in incident energy, where the incident energy of single-electron loss is less than 6.3 keV/a.u., and the incident energy of double-electron loss is less than 1.6 keV/a.u. This may be due to the fact that the local density approximation cannot adequately describe the electron correlation effect in the low-energy region. Our results are in good agreement with the available experimental data up to the five-fold electron loss cross-section, and for scenarios in which $m > 5$, the values of these sections are too small to be accurately measured, and are excluded in this figure. Privovar *et al.*[33] confirmed that with an increase in m, the slope of the electron-loss curve will increase, which suggests that the process of multiple electron loss is more sensitive to incident energy.

As regards the total electron loss cross-section ($\sigma_{\rm tot} = \sum_{m=1}^{7} \sigma_m^{\rm loss}$), compared with the theoretical results of Shevelko *et al.*,[37] our data are in better agreement with the experiment of Privovar *et al.* when the incident energy is greater than 1.6 keV/a.u., and the change in cross-section with impact energy is unnoticeable, apart from the uptrend between 6.3 keV/a.u. and 10 keV/a.u. With the increase in impact energy, the interaction between particles is enhanced, while the interaction time is reduced, due to the increase in the speed of the impact particle, which weakens the effect of the impact energy. At 1.6 keV/a.u., our result is much higher than that of Shevelko *et al.*, which indicates that local density approximation may be inadequate to quantitatively describe low-energy electronic dynamics.

As the incident energy increases, the electron loss cross-section is increased, and the electron capture cross-section decreases. In addition, the single-electron loss cross-section is larger than the single-electron capture cross-section. This phenomenon confirms that the process of electron capture occurs in the range of lower incident energy, while the electron loss process is more likely to take place in the range of relatively higher incident energy; the electron loss process is of great importance across the whole range of incident energy studied in this work.

In order to learn more about the cross-sections, single-electron capture probabilities ($2\pi P_n^{\rm cap} b$, $n = 1$)

are shown in Fig. 4(a), and electron-loss probabilities ($2\pi P_m^{\rm loss} b$, $m = 1, \ldots, 5$) at five different incident energies of 45, 25, 10, 6.3, and 1.6 keV/a.u. are given in Figs. 4(b)–4(f). The target region covers the whole computational space.

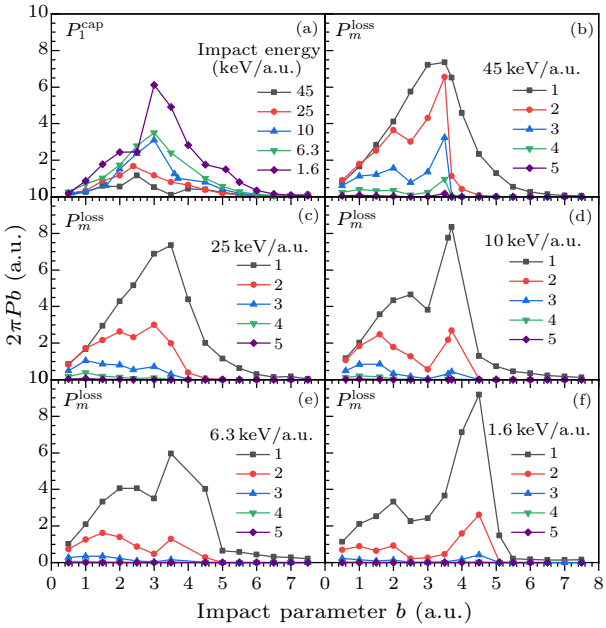

Fig. 4. The probability of single electron capture, and the probability of single-electron loss and multi-electron loss vary with the impact parameters at incident energy levels of 45, 25, 10, 6.3, and 1.6 keV/a.u. The numbers in the legend of in (a) represent the value of the incident energy in keV/a.u., and for (b)–(f), the numbers in the legend represent the number of lost electrons.

Figure 4(a) shows the single-electron capture (SEC) probability as a function of impact parameter at different incident energies. Note that the capture of more than two electrons is a weak process, which is usually negligible in experiments. With regard to the process of single-electron capture, we note that with an increase in impact energy, the probability will decrease, and the peak position will move towards smaller impact parameters, which suggests that the electron-capture process is more likely to occur in a relatively low-energy region.

The electron-loss probabilities decrease if more electrons are lost under the same incident energy and impact parameters. In most cases, there are two peaks on the electron-loss probability curves, apart from single-electron loss probabilities at impact energy levels of 45 keV/a.u. and 25 keV/a.u., and the peak positions show a tendency to appear at small impact parameters with an increase in the electron loss number. For each $2\pi P_m^{\rm loss} b$, the single-electron loss is the dominant process; we find that the single-electron loss cross-sections, particularly in the peak regions, do not critically depend on the impact energy. However, for 2–3 electron loss probabilities, $2\pi P_{m=2,3}^{\rm loss} b$, we observe an overall enhancement as impact energy increases; for example, the $2\pi P_{m=2}^{\rm loss} b$ at 45 keV/a.u. is larger than that at 1.6 keV/a.u. by approximately a factor of two.

Comparing the situation of electron loss and electron capture, the probability of electron loss and the probability of electron capture mainly occur in regions with smaller impact parameters, and the maximum electron-loss probability occurs between $3.5a_0$ to $4.5a_0$, while the maximum electron-capture probability occurs between $2.5a_0$ and $3a_0$, which means that the electron loss and electron capture processes are both close collisions, and the electron capture process occurs more readily at smaller impact parameters than the electron-loss process. When the impact parameter is greater than $7.5a_0$, almost all the probabilities of electron loss and electron capture converge to zero, and the probabilities of electron loss decrease more rapidly with the increase in the number of electrons lost. This also suggests that the range of impact parameter we select is sufficient to calculate the cross-sections, and, more importantly, that the multiple-electron loss process is more sensitive to impact parameters.

In summary, we have studied the collision processes of Ar^+–Ne collision in the impact energy region of 1.6–45 keV/a.u. by means of a time-dependent density functional theory, together with molecular dynamics. The calculated single-electron capture and 2–4 electron loss cross-sections agree with experimental data for the relevant energy region. The electronic dynamics, illustrated by the spatial distributions of electronic density, reveal a non-negligible ionization of the Ar^+ ion after collision, resulting in a decrease in electron capture probabilities, and an increase in electron loss probabilities over hundreds of femtoseconds. In addition, the electron-loss probabilities clearly show that the electron-loss process prefers high-impact energies, and a substantial ionization of the Ar ion is observed. Our work also highlights the inadequacies of the current local density functional when applied to low impact energies; as such, to address Ar^+–Ne collision effectively, more advanced methods will need to be developed in the future.

References

[1] Aumayr F, Ueda K, Sokell E, Schippers S, Sadeghpour H, Merkt F D R, Gallagher T F, Dunning F B, Scheier P, Echt O, Kirchner T, Fritzsche S, Surzhykov A, Ma X, Rivarola R, Fojon O, Tribedi L, Lamour E, Crespo L U J R, Litvinov Y A, Shabaev V, Cederquist H, Zettergren H, Schleberger M, Wilhelm R A, Azuma T, Boduch P, Schmidt H T and Stöhlker T 2019 *J. Phys. B: At. Mol. Opt. Phys.* **52** 171003

[2] Tolstikhina I, Imai M, Winckler N and Shevelko V 2018 *Basic Atomic Interactions of Accelerated Heavy Ions in Matter* (Springer Series on Atomic, Optical and Plasma Physics) (Berlin: Springer)

[3] Isler R C 1994 *Plasma Physics Controlled Fusion* **36** 171

[4] Niemann H B, Atreya S K, Bauer S J, Carignan G R, Demick J E, Frost R L, Gautier D, Haberman J A, Harpold D N, Hunten D M, Israel G, Lunine J I, Kasprzak W

T, Owen T C, Paulkovich M, Raulin F, Raaen E and Way S H 2005 *Nature* **438** 779
[5] Lisse C M, Dennerl K, Englhauser J, Harden M, Marshall F E, Mumma M J, Petre R, Pye J P, Ricketts M J, Schmitt J, TrCumper J and West R G 1996 *Science* **274** 205
[6] Liang G Y, Peng Y G, Li R, Wu Y and Wang J G 2020 *Chin. Phys. Lett.* **37** 123101
[7] Amaldi U and Kraft G 2005 *Rep. Prog. Phys.* **68** 1861
[8] Matthew B, Tom K and Engel E 2017 *Phys. Rev. A* **96** 032708
[9] Ullrich J, Moshammer R, Dörner R, Jagutzki O, Mergel V, Böcking H S and Spielberger L 1997 *J. Phys. B: At. Mol. Opt. Phys.* **30** 2917
[10] Ermolaev A M 1990 *Phys. Lett. A* **149** 151
[11] Toshima N 1993 *Phys. Lett. A* **175** 133
[12] Kirchner T, Gulyás L, Lüdde H J, Henne A, Engel E and Dreizler R M 1997 *Phys. Rev. Lett.* **79** 1658
[13] Lüde HJ, Horbatsch M, Henne A and Dreizler R M 1990 *Phys. Lett. A* **145** 173
[14] Fainstein P D, Ponce V H and Rivarola R D 1988 *J. Phys. B: At. Mol. Opt. Phys.* **21** 287
[15] Schenk G and Kirchner T 2015 *Phys. Rev. A* **91** 052712
[16] Kirchner T and Horbatsch M 2001 *Phys. Rev. A* **63** 062718
[17] Kirchner T, Horbatsch M and Lüdde H J 2004 *J. Phys. B: At. Mol. Opt. Phys.* **37** 2379
[18] Fritsch W and Lin C D 1991 *Phys. Rep.* **202** 1
[19] Zapukhlyak M, Kirchner T, Lüdde H J, Knoop S, Morgenstern R and Hoekstra R 2005 *J. Phys. B: At. Mol. Opt. Phys.* **38** 2353
[20] Imai T W, Kimura M, Gu J P, Hirsch G, Buenker R J, Wang J G, Stancil P C and Pichl L 2003 *Phys. Rev. A* **68** 012716
[21] Wang K, Wang X X, Qu Y Z, Liu C H, Liu L, Wu Y and Buenker R J 2020 *Chin. Phys. Lett.* **37** 023401
[22] Gao J W, Wu Y, Wang J G, Sisourat N and Dubois A 2018 *Phys. Rev. A* **97** 052709
[23] Runge E and Gross E K U 1984 *Phys. Rev. Lett.* **52** 997
[24] Ullrich C A 2012 *Time-Dependent Density-Functional Theory: Concepts and Applications* (Oxford: Oxford University Press)
[25] Wang F, Hong X, Wang J and Kim K S 2011 *J. Chem. Phys.* **134** 154308
[26] Hong X, Wang F, Wu Y, Gou B and Wang J 2016 *Phys. Rev. A* **93** 062706
[27] Bi G, Kang J and Wang L W 2017 *Phys. Chem. Chem. Phys.* **19** 9053
[28] Wang Z P, Zhang F S, Xu X F and Qian C Y 2020 *Chin. Phys. B* **29** 023401
[29] Thierry L, Katia C, Holtzman J and Hubeny I 2008 *Astrophys. J.* **678** 1342
[30] Deutsch H, Becker K, Grum-Grzhimailo A N, Bartschat K, Summers H, Probst M, Matt-Leubner S and Märk T D 2004 *Int. J. Mass Spectrom.* **233** 39
[31] Ton-That D and Flannery M R 1977 *Phys. Rev. A* **15** 517
[32] Zhu X M and Pu Y K 2010 *J. Phys. D: Appl. Phys.* **43** 403001
[33] Pivovar L I, Novikov M T and Dolgov A S 1966 *Sov. Phys. JETP* **23** 357
[34] DuBois R D, Santos A C F, Olson R E, Stöhlker T, Bosch F, Bräuning-Demian A, Gumberidze A, Hagmann S, Kozhuharov C, Mann R, Muthig A O, Spillmann U, Tachenov S, Barth W, Dahl L, Franzke B, Glatz J, Gröning L, Richter S, Wilms D, Krämer A, Ullmann K and Jagutzki O 2003 *Phys. Rev. A* **68** 042701
[35] Olson R E, Watson R L, Horvat V and Zaharakis K E 2002 *J. Phys. B: At. Mol. Opt. Phys.* **35** 1893
[36] Olson R E, Watson R L, Horvat V, Perumal A N, Peng Y and Stöhlker T 2004 *J. Phys. B: At. Mol. Opt. Phys.* **37** 4539
[37] Shevelko V P, Kato D, Litsarev M S and Tawara H 2010 *J. Phys. B: At. Mol. Opt. Phys.* **43** 215202
[38] Ullrich C A, Reinhard P G and Suraud E 2000 *Phys. Rev. A* **62** 053202
[39] Calvayrac F, Reinhard P G, Suraud E and Ullrich C A 2000 *Phys. Rep.* **337** 493
[40] Maitra N T 2016 *J. Chem. Phys.* **144** 220901
[41] Reinhard P G and Suraud E 2003 *Introduction to Cluster Dynamics* (New York: Wiley)
[42] Andrade X, Alberdi-Rodriguez J, Strubbe D A, Oliveira M J, Nogueira F, Castro A, Muguerza J, Arruabarrena A, Louie S G, Aspuru-Guzik A, Rubio A and Marques M A 2012 *J. Phys. Condens Matter* **24** 233202
[43] Tavernelli I, Gaigeot M P, Vuilleumier R, Stia C, Herve D P M A and Politis M F 2008 *ChemPhysChem* **9** 2099
[44] Avendaño-Franco G, Piraux B, Grüning M and Gonze X 2012 *Theor. Chem. Acc.* **131** 1289
[45] Yu W, Zhang Y, Zhang F S, Hutton R, Zou Y, Gao C Z and Wei B 2018 *J. Phys. B: At. Mol. Opt. Phys.* **51** 035204
[46] Yu W, Gao C Z, Zhang Y, Zhang F S, Hutton R, Zou Y and Wei B 2018 *Phys. Rev. A* **97** 032706
[47] Yu W, Gao C Z, Jiang T, Zou Y, Wang J G, Wu Y and Wei B 2019 *J. Chem. Phys.* **150** 124304
[48] Bates D R and McCarroll R 1958 *Proc. R. Soc. London. Ser. A.* **245** 175
[49] Vignale G 1995 *Phys. Rev. Lett.* **74** 3233
[50] Yu W, Gao C Z, Sato S A, Castro A, Rubio A and Wei B 2021 *Phys. Rev. A* **103** 032816
[51] Castro A, Appel H, Oliveira M, Rozzi C A, Andrade X, Lorenzen F, Marques M A L, Gross E K U and Rubio A 2006 *Physica Status Solidi (b)* **243** 2465
[52] Wang Z, Li S S and Wang L W 2015 *Phys. Rev. Lett.* **114** 063004
[53] Marques M A L,Castro A, Bertsch G F and Rubioa A 2003 *Comput. Phys. Commun.* **151** 60
[54] Perdew J P and Zunger A 1981 *Phys. Rev. B* **23** 5048
[55] Schlipf M and Gygi F 2015 *Comput. Phys. Commun.* **196** 36
[56] Gomez P A, Marques M A L, Rubio A and Castro A 2018 *J. Chem. Theory Comput.* **14** 3040
[57] Castro A, Marques M A L and Rubio A 2004 *J. Chem. Phys.* **121** 3425
[58] Kołakowska A, Pindzola M S, Robicheaux F, Schultz D R and Wells J C 1998 *Phys. Rev. A* **58** 2872
[59] Wittkower A B and Gilbody H B 1967 *Proc. Phys. Soc* **90** 353